Hybrid Energy Production Analysis and Modelling for Radio Access Network Supply

Greta Vallero[a] and Michela Meo[b]

Department of Electronics and Telecommunications, Politecnico di Torino, Italy

Abstract: To move towards sustainability, Renewable Energy Sources (RES) have started to partially substitute fossil fuels based energy generation. Also for the Information and Communication Technology (ICT) ecosystem supply, and in particular in the Radio Access Networks (RANs), the usage of PV panels has been considered an effective solution. Since the communication infrastructure has to be powered continuously, to face the problem of the absence of the Photovoltaic (PV) panel energy production during the night, we consider a hybrid solution, composed by a PV panel and a wind turbine, for the supply of Base Stations (BSs). Starting from the characterisation of wind energy production, we assess the impact of the employment of the combination of these RES on the excesses and deficits of energy production, highlighting that the hybrid solution better fits the BS energy demand. In order to predict performance, we build polynomial models, which highlight the effects of the variation of the installed wind and solar capacities.

1 INTRODUCTION

In order to comply with the Paris Agreement and the European Green Deal, the electricity system has begun a transition towards a more sustainable production process (Commission, 2019). As a result, the production share of fossil fuels has started reducing, while a large RES penetration has been planned in the next years. This is the response to achieve climate goals, while facing the growth of the electricity demand, which is supposed to maintain, until 2040, its current increasing rate of 2.1% per year (IEA, 2020). Besides the sustainability issues, this transformation is also motivated by the petrol shock crisis, which will occur at the end of the "post-peak" period, in which we are entering (Hirsch, 2008). This "post-peak" period starts after the peak oil moment, which occurs at the maximum oil production phase. After this, the oil production declines, causing energy price growth and important economical implications. As a result, in 2019, renewable electricity generation rose by 6%, and 64% of this 6% derived from the installation of new wind turbines and solar energy generators, which are supposed to be further expanded to reach half of

the electricity generation by 2030 (IEA, 2020). Also the supply of the ICT sector, responsible for 3% of the CO_2 emissions in 2018 and, according to forecasts, up to 14% in 2040, has been involved in this transformation (Belkhir and Elmeligi, 2018). The European Commission, in (Bertoldi, 2017), under the need for actions to improve the energy efficiency in communications, has formalised a policy for the regulation of the energy consumption and the carbon emissions of the Broadband Communication Equipment. Meanwhile, the communication community has recognised the network energy efficiency as a fundamental and urgent aspect. As well known, the BSs have been identified as the most energy consuming components of mobile networks (Gati et al., 2019), accounting for 80% of the total energy consumption of the Radio Access Networks (RANs). The BSs energy consumption is expected to further grow because of the rise of the mobile IP traffic, which will reach 77.5 exabyte (EB) per month by 2022 and 5 016 EB per month in 2030 (Gati et al., 2019; Forecast, 2019; Tariq et al., 2020), more than, respectively, 6 and 400 times larger than 11.5 EB per month occurred in 2017. To address these issues, the usage of PV panel systems for the supply of BSs, installed in proximity to these infrastructures, has been becoming an attractive solution (Chamola and Sikdar, 2016; Hassan et al., 2013;

[a] https://orcid.org/0000-0002-6420-231X
[b] https://orcid.org/0000-0001-7403-6266

131

Han and Ansari, 2014; Deruyck et al., 2017). Indeed, besides the improvement of the RAN sustainability, it is a promising approach to make the network more independent from the power grid, as well as to reduce the network electricity bill, which is the key contributor for the increase of the Operational Expenditure (OPEX) (Renga and Meo, 2019; Pompili et al., 2016). Because of this, 390 000 newly solar powered BSs have been installed worldwide since 2012, at an annual rate of 84 000 solar powered BS per year, 6 times higher with respect to 2012 and their usage is expected to significantly advance in 6G RANs (Res., 2013; Smertnik et al., 2014; Tariq et al., 2020). The authors of (Deruyck et al., 2017) and (Aktar et al., 2018) consider a PV panel system to reduce the CO_2 emissions used to generate energy by burning fossil fuels, when powering a RAN; in (Guo et al., 2019) a wind turbine system is considered for the same purpose.

While the solution is promising, various issues need to be addressed, among which the solar panel dimensioning and the possible lack of energy generation due to its intermittent nature. Indeed, the solar energy harvesting presents, as other RESs, randomness, dependence on the weather conditions and daily and seasonal variability, making these BSs self-survival unstable. To tackle these issues, it is fundamental to combine different renewable energy sources. In this work, we consider the combination of wind and solar RES for the supply of a BS, so as to exploit their operating characteristics and to achieve higher efficiency than the one that could be obtained from a single energy source. In particular, in the first part of our work, we analyse a data-set, which reports real data of the energy production of wind turbines and PV panel systems, installed in Belgium. Then, we simulate a single BS, powered by an hybrid system, composed by a PV panel and a wind turbine, using real mobile traffic demand and energy production data. This scenario is evaluated in terms of energy performance, expressed as annual bought energy and annual wasted energy. Finally, models for the prediction of this energy performance are proposed, as a function of the installed capacity of the wind and solar energy generators, in order to properly design the energy system for future RANs.

2 DATA SET

In this work, we use the energy production data provided by the Open Power System Data (OPSD) project (Data, 2020). This data-set contains different kinds of time series, such as onshore and off-
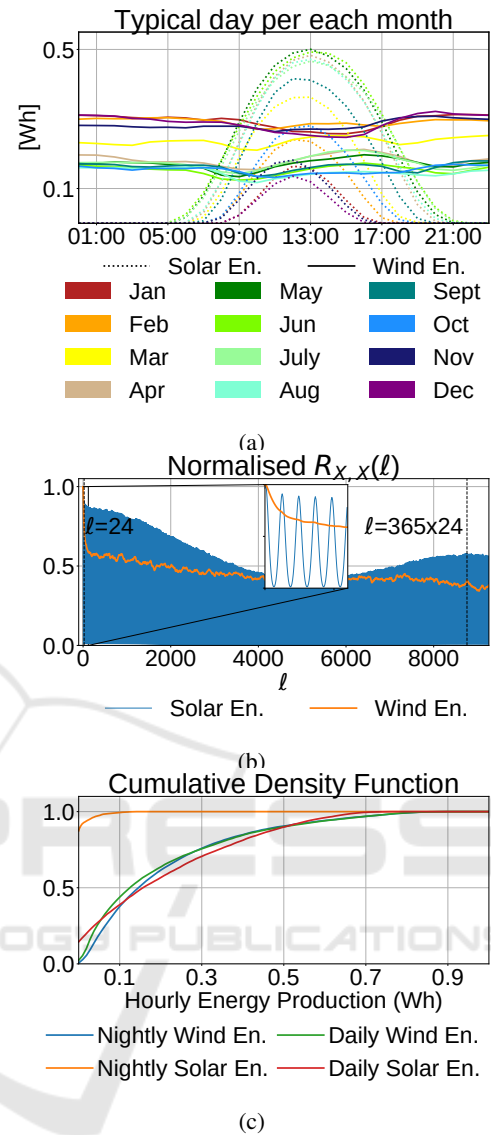

Figure 1: Characterisation of the Belgian wind and solar energy production: (a) Daily wind and solar energy production in each month, (b) Normalised Auto-correlation function $R_{X,X}(\ell)$ of the wind and solar energy production, (c) Cumulative Density Function of the daily and nightly wind and solar energy production.

shore wind power generation, solar power generation, installed wind and solar capacities, electricity prices and electricity consumption, for 37 European countries from 2012 to 2017. All variables are provided in hourly resolution, but some of them are also available in higher resolution (half-hourly or quarter-hourly). The data-set has been created by downloading the data of interest from the sources, i.e, from the Transmission System Operators (TSOs) of the different countries, resampling and merging them in a large CSV file.

Because of lack of some data, we select data from 01/01/2015 to 31/12/2017 of Belgium, Switzerland, Germany and Denmark with hourly granularity and we consider the *actual wind energy production on-shore*, *actual solar power production*, *wind monitored capacity* and *solar monitored capacity* fields, which are reported in MW. Each production data is normalised by the corresponding monitored capacity, in order to compute the wind and solar power, in W, which is produced by, respectively, a turbine and PV panel system whose capacity is 1 W. Then, the hourly energy produced by a wind/solar capacity of 1 W is computed, in *Wh*.

3 WIND ENERGY PRODUCTION DATA

In this section, we discuss the characterisation of the Belgian wind energy production as derived from the used data-set. As mentioned in Sec. 2, it collects the wind energy production, as well as the solar one, and their corresponding installed capacity, registered between 2015 and 2017. We use these data to highlight similarities and differences between solar and wind energy production. In Fig. 1a, the typical energy production day in each month is plotted. In particular, plain and dashed lines indicate the mean hourly wind and solar production, respectively, for each month. First, we notice that, as largely discussed in (Hadji et al., 2018; Renga et al., 2018), the solar generation strictly depends on the presence of the sun. As a consequence, a PV panel system produces energy only for a limited amount of hours, which significantly varies with the seasons, from 18 hours in June to 9 hours in December. This does not occur for the wind energy: results suggest that a wind turbine system produces for the whole duration of the day and its production is almost constant during the day. Moreover, the solar energy production peaks are much larger in summer than in winter: they are around 0.5Wh in May, when the maximum is reached, while no larger than 0.13 Wh in December, corresponding to the minimum peak, resulting in a drop by 73%. Quite the opposite occurs for the wind energy production: January, February, November and December, respectively, in red, orange, blue and purple in the figure, present the largest values for the wind energy production.

The auto-correlation functions $R_{X,X}(\ell)$ of the solar and wind energy production are reported in Fig. 1b, in blue and orange, respectively. From this figure, it is evident that the solar energy production is characterised by a daily periodicity (see blue curve in the
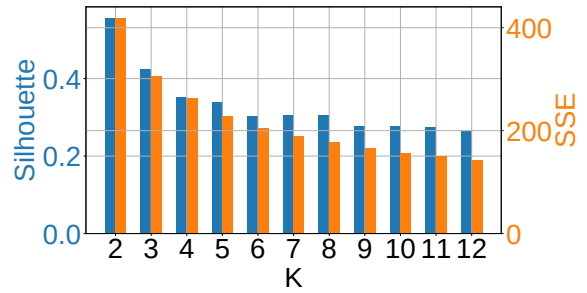

Figure 2: Silhouette index (left-y-axis, in blue) and SSE index (right-y-axis, in orange) for different values of K.

zooming rectangle of Fig. 1b), as indicated by the visible peaks when ℓ of the auto-correlation is 24 or a multiple of it. The presence of the peak when ℓ is 8760 means the presence of a seasonal periodicity in the pattern. These are not the cases of the wind energy generation. The orange curve in the figure indicates the absence of any periodicity in the pattern and suggests the high level of randomness of the wind energy production.

Fig. 1c shows the Cumulative Distribution Functions (CDFs) of the hourly wind and solar energy production during the day, i.e. from 8 a.m. to 8 p.m. and during the night, i.e. from 8 p.m. to 8 a.m.. The curves, which correspond to the daily and nightly wind energy production and to the daily solar production, are similar and reach 1 around 0.65 Wh. Meanwhile, as indicated by the figure, the hourly solar production during the night is always lower than 0.05 Wh. This highlights again the different variation within the daily pattern, provided by the two energy sources. Moreover, contrary to the hourly solar energy production, the hourly wind production is close to zero with infinitesimal probability.

3.1 Clustering

In order to explore the daily wind energy production and extract typical daily patterns, the *K-means* clustering algorithm is employed. We consider as an observation the daily pattern of hourly wind energy generation; i.e., a vector of 24 elements where each element is the energy production in a given hour of a day. The *K-means* partitions the observations into K clusters in which each observation belongs to the cluster with the nearest mean, i.e. the nearest centroid, so as to minimise the within-cluster variance. In particular, the K-means algorithm starts with K random centroids, and then performs iterative calculations to optimise the positions of these centroids, until they stabilise. In each iteration, the *assignment step* and the *update step* are performed. In the assignment step, each observation is assigned to the cluster with the
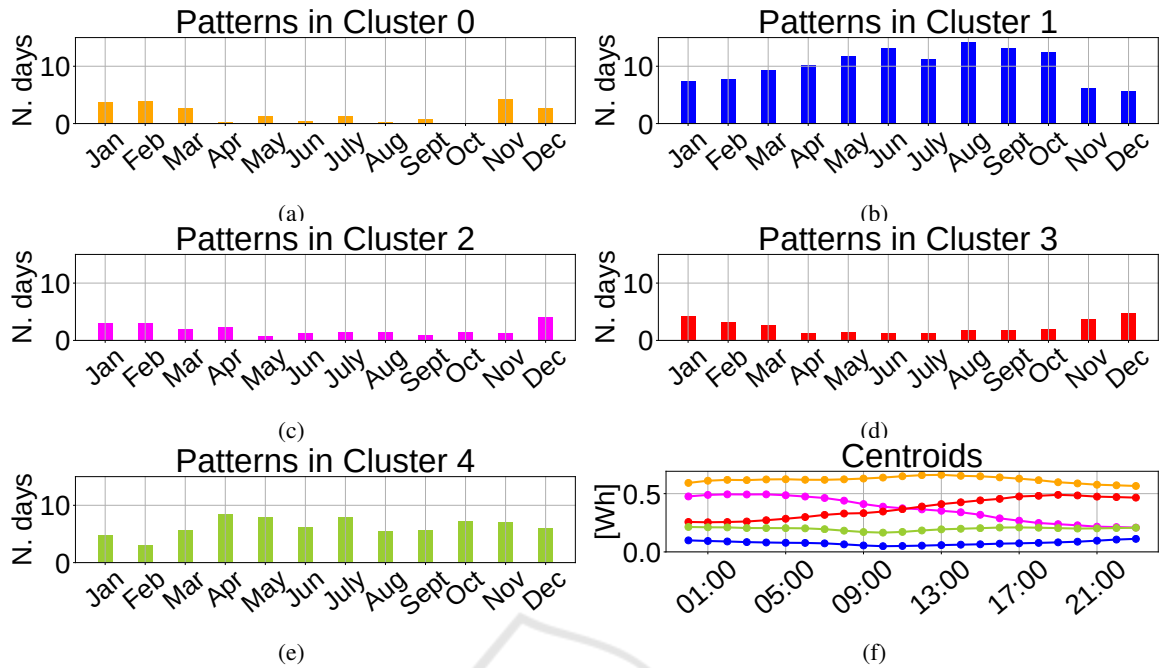
Figure 3: Results of the clustering with K=5: (a)-(e) number of observations clustered in each cluster, (f) resulting centroids.

nearest mean. The update step recalculates the centroid of each cluster, as the mean of the observations assigned to that cluster. Since the performance of the algorithm depends on the random initialisation of the centroids, the algorithm is performed 100 times with different random seeds.

We perform this procedure for the numbers of clusters K, varying between 2 and 12. Then, we select the K solution, using the *Elbow method* (Bholowalia and Kumar, 2014; Kodinariya and Makwana, 2013). According to it, the optimal number of clusters is indicated by the elbow of the curve of the Sum of the Squared Error (SSE), or distortions, and of the Silhouette parameter (Petrovic, 2006; Desgraupes, 2013). The SSE is the sum of distance of each observation, i.e., a daily wind energy production pattern in our case, from the centroid of the cluster it belongs; the Silhouette parameter provides a measure of how close an observation is from its centroid, compared to the distance from the others. Fig.2, where the Silhouette and Distortion indexes are plotted in blue and orange, respectively, indicates that the best choice for K is 5. Figure 3 illustrates the results of the clustering with K equals to 5. In particular, in Fig. 3f, each curve corresponds to the centroid of each of the 5 clusters, while Figs. 3a-3e report, for each cluster, the number of daily patterns, in each month, assigned to the corresponding cluster; the colours of the distributions of points in clusters are the same used for the centroids. Fig. 3f highlights that the algorithm identifies a cluster, characterised by a very low daily energy produc-

Table 1: Values of the parameters of the consumption model for macro and small cell BSs.

BS type	N_{trx}	P_{max} (W)	P_0 (W)	Δ_p
Macro	6	20	84	2.8

tion, never larger than 0.12 Wh, (blue curve in the figure, corresponding to cluster 1) and another, plotted in green in the figure (Cluster 4), when the production is larger, between 0.17 and 0.22 Wh. Significant higher values are reached by the centroids plotted in yellow, red and pink. For these clusters, these large production values, always larger than 0.22 Wh and up to 0.66 Wh, are reached during the first part of the day (see pink curve in Fig. 3f), in the last part, as for the red curve in Fig. 3f, or for the whole duration of the day (see yellow curve in Fig. 3f). From Figs. 3a-3e, we notice that the largest part of patterns belong to the clusters, whose centroid is characterised by the lowest daily wind energy production (i.e. blue and green curves in Fig. 3f). On the contrary, the clusters, whose centroid reaches a large amount of produced energy during part of the day (see pink and red curves in Fig. 3f), or for the whole duration of the day (yellow curve in Fig. 3f), have few patterns and those patterns occur typically during the winter months, i.e. January, February, November and December, while summer is characterised by low production levels.

4 SIMULATION SET UP

In this part of the work, we consider a single macro cell BS of a RAN, supplied by a hybrid system, with total capacity C_{tot}, in kW, composed by a wind turbine, whose capacity is W, in kW, and a PV panel system, with capacity S, in kW, and the grid. Data provided by a large Italian mobile network operator are used in this study. They report the traces of the traffic demand volume, in bits, of numerous BSs located in Milan, Italy, for two months in 2015, with granularity of 15 minutes. The traffic traces are aggregated to derive an hourly granularity and they are averaged in order to obtain the typical daily traffic demand of each BS, with an hourly granularity. For our work, two different traces are selected, corresponding to BSs, located in different areas of the city, in order to consider samples of quite different scenarios, and, hence, traffic patterns, which are representative of the various zones that coexist in an urban environment. First, a BS located in proximity of the train station area is selected. It is characterised by intense activity levels, especially at the beginning and at the end of the working hours. The second BS is picked in the San Siro district, which includes a large soccer stadium, meaning that the activity here is variable depending on the scheduled matches and concerts, resulting very heavy when these events occur.

The input power required for the operation of a BS in an hour, denoted as $E_{in}^{(t)}$, in Wh, is derived according to the linear model proposed in (Auer et al., 2010):

$$E_{in}^{(t)} = N_{trx} \cdot (P_0 + \Delta_p P_{max} \rho), \qquad 0 \leq \rho \leq 1 \quad (1)$$

where N_{trx} is the number of transceivers, P_0 represents the power consumption when the radio frequency output power is null, Δ_p is the slope of the load dependent power consumption, ρ is the traffic load and P_{max} is the maximum radio frequency output power at maximum load. Table 1 summarises the value of the parameters for a macro cell BSs (Auer et al., 2010).

As already mentioned, the considered BS is supplied by an hybrid RES system, composed of a PV panel and a wind turbine. The Belgian data for the wind and solar energy, generated by, respectively, a wind turbine and a PV panel, located in Belgium, are used, taken from (Data, 2020) and presented in section 2. As mentioned above, the data-set provides the amount of Watt produced by a PV panel and a wind turbine, both with capacity of 1 W. In order to derive the energy generated by the simulated RES system, we multiply these data by their capacity, expressed in Watt.

In our simulations, we assume that each considered BS operates for 3 years. The BS uses the green

power generated by the RESs and when the energy production exceeds the BS consumption, that amount of energy is wasted. In case the generated energy is not enough to power the BS, the missing energy is bought from the grid. In each time slot, which lasts 1 hour, the BS energy consumption $E_{in}^{(t)}$ is computed, as in (1), and, knowing the energy that is generated by the supply system, $E_{pr}^{(t)}$, during that time slot, the bought and wasted energy are computed. The bought energy $E_b^{(t)}$ measures the amount of energy, in Wh, which is bought from the grid during that time slot, when the RES system does not produce enough energy for the BS supply; the wasted energy $E_w^{(t)}$ provides the total energy, in Wh, which exceeds the BS energy consumption and so it is not used. They are given by:

$$E_b^{(t)} = max(0, E_{in}^{(t)} - E_{pr}^{(t)}) \quad (2)$$

$$E_w^{(t)} = max(0, E_{pr}^{(t)} - E_{in}^{(t)}) \quad (3)$$

where $E_{in}^{(t)}$ is the energy consumed at time t, computed as in (1), $E_{pr}^{(t)}$ is the energy produced by the power supply system at time t

Once a simulation is completed, the following energy metrics are computed:

- E_b: it is the average amount of energy, measured in Wh/year, which is bought from the grid every year. It is computed as follows:

$$E_b = \frac{1}{Y} \sum_{t=0}^{Y \cdot 365 \cdot 24} E_b^{(t)} \quad (4)$$

where $E_b^{(t)}$ is the energy bought from the grid at time t, computed as in (2) and Y is the number of considered years.

- $E_{b,h}$: it accounts for the bought energy, in Wh/year, at hour h, with $h = 0, 1, 2, .., 23$, in each year. It is given by:

$$E_{b,h} = \frac{1}{Y} \sum_{\substack{t=0 \\ t\%24=h}}^{Y \cdot 365 \cdot 24} E_b^{(t)} \quad (5)$$

where, as above, $E_b^{(t)}$ is the energy bought from the grid at time t (see (2)) and Y is the number of considered years.

- E_w: it provides the annual wasted energy, in Wh/year:

$$E_w = \frac{1}{Y} \sum_{t=0}^{Y \cdot 365 \cdot 24} E_w^{(t)} \quad (6)$$

where, $E_w^{(t)}$ is the wasted energy in time slot t, derived as in (3) and Y is the number of considered years.

- $E_{w,h}$: it measures the amount of wasted energy, in Wh/year, at hour h, with $h = 0, 1, 2, .., 23$, in each year. It is computed as:

$$E_{w,h} = \frac{1}{Y} \sum_{\substack{t=0 \\ t\%24=h}}^{Y \cdot 365 \cdot 24} E_w^{(t)} \qquad (7)$$

where, as above, $E_w^{(t)}$ is the wasted energy at time t, computed as in (3) and Y is the number of considered years.

5 SIMULATION RESULTS

In this section, we discuss the results of the simulations, using the metrics presented above. Besides the impact of the total installed RES capacity C_{tot} on these metrics, we also investigate the impact of its distribution between the PV panel capacity, S, and the wind turbine capacity, W. In particular, we consider C_{tot} equal to 1 kW, 4 kW and 5 kW and we vary its distribution among the solar and wind energy generator systems. The results are compared with our benchmark, i.e., the scenario in which no RES is used and the electricity needed for the BS supply is totally taken from the grid. This means that E_b is equal to the annual BS energy consumption, which is, according to our simulations, 5.1 MWh for San Siro BS and 5.6 MWh for the Train Station BS; E_w is 0 MWh.
In Fig. 4, E_w and E_b, in blue and orange, respectively, are plotted, for the Train Station BS, on the left, and the San Siro BS, on the right. Each row of the figure considers different total RES installed capacity: 1 kW, in Figs. 4a, 4b, 4 kW in Figs. 4c, 4d and 5 kW in Figs. 4e, 4f. On the left of each plot, only the solar capacity is used, while moving towards right, solar capacity diminishes by 0.5 kW and the capacity of the wind turbine grows of 0.5 kW at each step, i.e., at each group of bars. From Fig. 4, we first notice that E_b and E_w significantly vary with different C_{tot}. Indeed, the energy bought from the grid, E_b, decreases if the total capacity grows, from a maximum of 5.56 MWh, when C_{tot} is 1 kW, to a minimum of 0.93 MWh, when the capacity of RES is 5 kW. Similarly, when the C_{tot} becomes larger, the waisted energy, E_w, rises, from 0 MWh, when C_{tot} is 1 kW, to a maximum of 4.97 MWh with C_{tot} equals to 5 kW.
Results in Fig. 4 reveal that E_b and E_w are also affected by the different distributions of these capacities between the wind and solar systems. Indeed, given a fixed total capacity C_{tot}, if the portion of wind capacity grows, E_b decreases but E_w increases. When C_{tot} is 1 kW, the reduction of the E_b is 17% and 18% with respect to the chosen benchmark, in San Siro and Train

Station areas, respectively, if the capacity is totally used as PV panel capacity. Meanwhile, E_b reaches its minimum value, dropping up to 34%, if all the capacity is employed for the wind turbines. The situation is different when C_{tot} is larger. Indeed, when it is 4 kW, for each considered BS, the minimum E_b is reached when the wind and the solar capacities are, respectively, 3 kW and 1 kW. In this scenario, E_b drops by 74% and 76%, for the BS in the Train Station and San Siro areas, respectively. In this case, the annual E_w is 1.43 MWh/year and 1.22 MWh/year, respectively.
Each curve in Fig. 5b represents $E_{w,h}$, with $h = 1,2,...,24$, i.e., the total amount of energy which is wasted during a year at each hour of the day, for the Train Station BS, for different W and S combinations, given C_{tot} equal to 4 kW. Values of $E_{w,h}$ close to 0 MWh are given before 7.00 a.m. and after 7.00 p.m., for values of W lower than 1.5 kW, which implies S larger than 2.5 kW (see light green, orange and blue curves in Fig. 5b). This is because the PV panel is not producing in these hours and the small capacity of the wind turbine does not exceed in production for the BS supply. Between 7.00 a.m. and 7.00 p.m., the PV panel produces energy because of the sun's presence. In this period of the day, the case with W and S equal to 1.0 kW and 3.0 kW, respectively, provides the lowest $E_{w,h}$, among the scenarios with W and S, respectively, lower than 1.5 kW and larger than 2.5 kW. Quite the opposite occurs for E_b, h, , with $h = 1,2,...,24$, whose behaviour is plotted in Fig. 5a, for different combinations of W and S, when C_{tot} is equal to 4 kW, for the Train Station BS. For values of W larger than 2.5 kW and, consequently, S lower than 1.5 kW, $E_{b,h}$ is no larger than 0.08 MWh, before 8.00 a.m. and after 6.00 p.m., as denoted by the pink, grey and dark green curves in Fig. 5a. In the same time interval, if W is lower than 2.5 kW and S larger than 1.5 kW, $E_{b,h}$ increases up to z MWh. Between 8.00 a.m. and 6.00 p.m., because of the limited contribution from the PV panel when its capacity is not larger than 0.5 kW, E_b, h grows up to 0.1 MWh, making the scenario with solar and wind capacities equal to 3.0 kW and 1.0 kW the best in terms of E_b.
Nevertheless, as can be seen in Fig. 4c, if the turbine has capacity 2.5 kW and the PV panel 1.5 kW, the E_b drops by 73% and 75% with respect to the benchmark scenario, respectively, resulting therefore slightly larger than the previous case, where, as mentioned, up to 74% and 76% of reduction is achieved. Nevertheless, this reduces E_w by 16% and 14%. Similarly, when C_{tot} is 5 kW, the hybrid solution, with 4 kW of wind capacity and 1 kW of solar one provides the lowest amount of E_b, as can be noticed in Figs. 4e and 4f. It results no larger than 1.1 MWh/year, re-
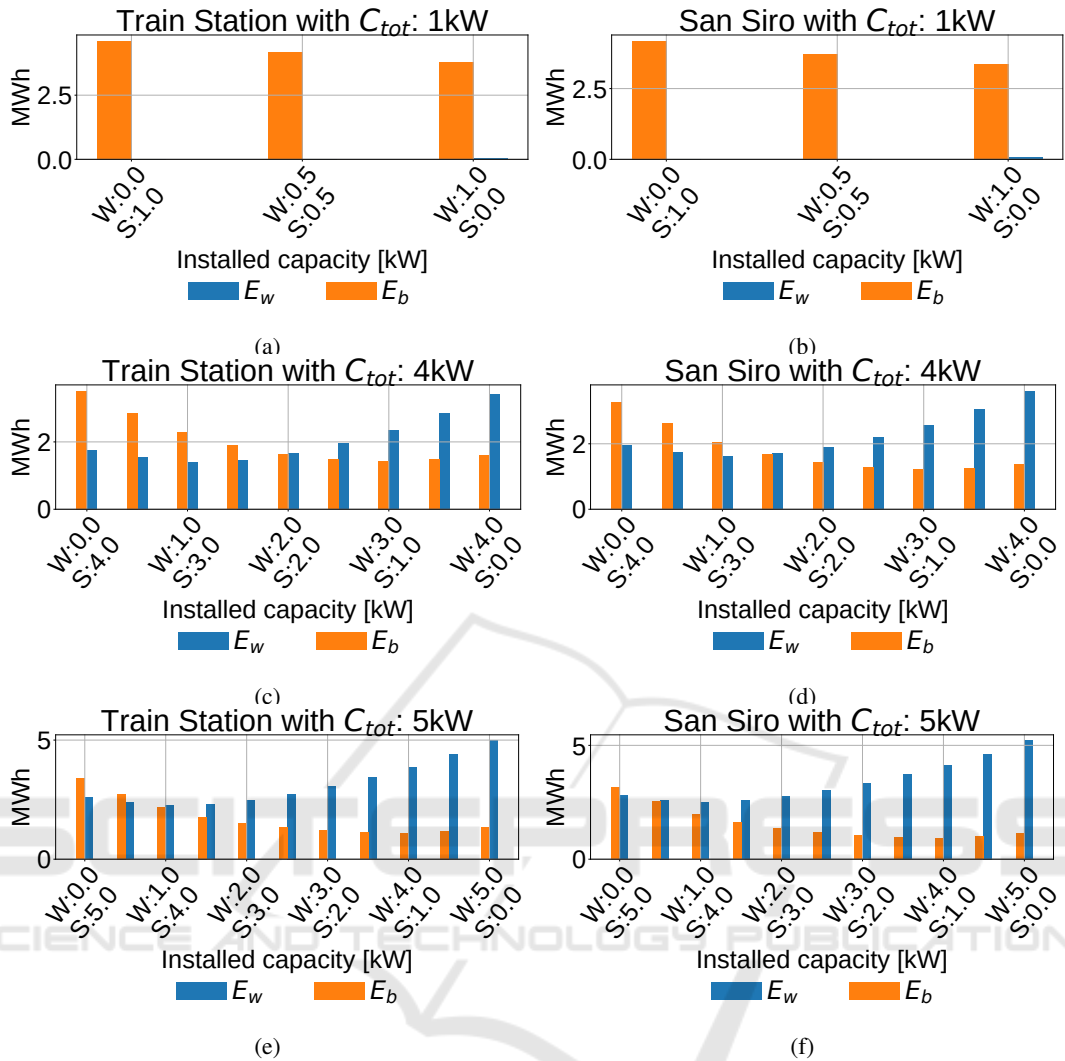
Figure 4: Simulations results: (a) E_b and E_w with C_{tot} equal to 1 kW for the Tran Station BS, (b) E_b and E_w with C_{tot} equal to 1 kW for the San Siro BS (c) E_b and E_w with C_{tot} equal to 4 kW for the Tran Station BS, (d) E_b and E_w with C_{tot} equal to 4 kW for the San Siro BS, (e) E_b and E_w with C_{tot} equal to 5 kW for the Tran Station BS, (f) E_b and E_w with C_{tot} equal to 5 kW for the San Siro BS.

duced by more than 80% with respect to our benchmark, but with an amount of wasted energy larger than 3.8 MWh/year. In order to reduce this by 26% for the Train Station BS and by 19% for the San Siro one, we employ a wind turbine with a capacity of 3 kW and a PV panel, whose capacity is 2 kW, at the expense of a little rise of the E_b, still resulting lower than 76% of E_b in the benchmark scenario.

These results show that hybrid solutions reduce both E_b and E_w. Indeed, for what concerns E_b, the hybrid solution copes with the lack of energy production by PV panel during the night, thanks to the turbine production. Meanwhile, the employment of the PV panel provides a large support to the BS supply during the BS energy consumption peaks, which occur

Table 2: p-value for the energy performance metrics E_b, E_w and the different input parameters W and S.

	E_b	E_w
W	0.0	0.0
S	$3.0 \cdot 10^{-47}$	0.05

daily, during the PV panel generation periods. Focusing on E_w, the hybrid solutions avoid that the wind turbine energy production exceeds the consumption during the night, when the BS energy consumption reaches its minimum. Similarly, the hybrid solution prevents wasting energy during the day, during the PV panel production hours.

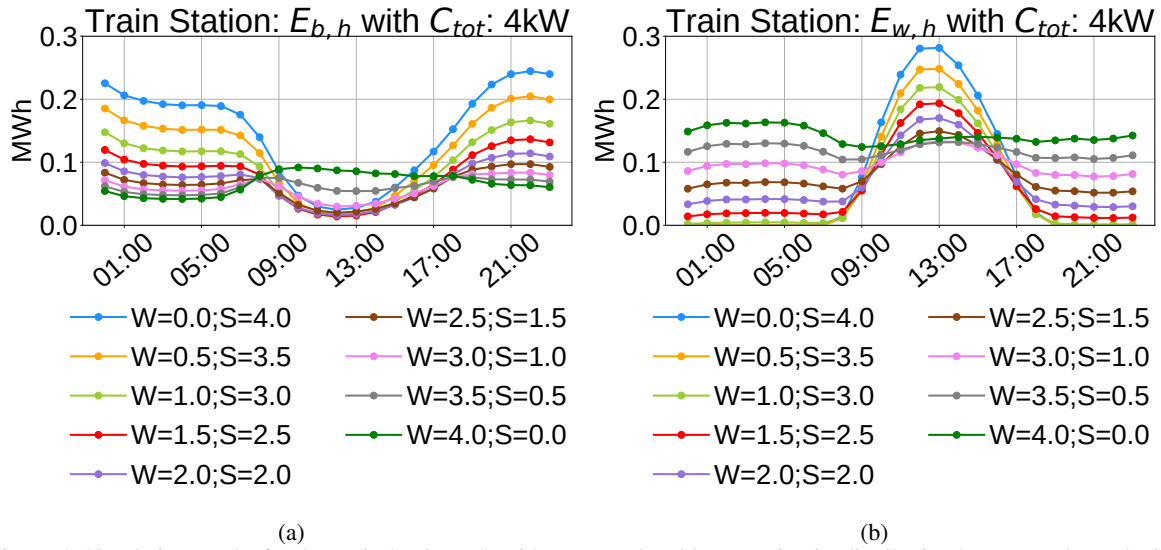(a)   (b)

Figure 5: Simulation results for the Train Station BS, with C_{tot} equal to 4 kW, varying its distribution between solar and wind capacity: (a) $E_{b,h}$, h=1,2,...,23 (b) $E_{w,h}$, h=1,2,...,23.

Table 3: Coefficients of the models for the prediction of E_b.

Country	a_b	b_b	c_b	d_b	e_b	K_b
Belgium	-831.33	-1582.29	0.09	0.10	0.16	$5 \cdot 10^6$
Denmark	-1697.26	-793.37	0.18	0.11	0.08	$5.12 \cdot 10^6$
Germany	-1617.87	-851.37	0.16	0.10	0.09	$5.23 \cdot 10^6$
Switzerland	-1525.72	-685.82	0.15	0.08	0.07	$5.30 \cdot 10^6$

6 PREDICTION MODEL

In this section, we propose two analytical prediction models to derive E_b and E_w, in different locations, namely, Belgium, Denmark, Germany and Switzerland. These models are based on the relation between E_b, E_w, in Wh, and the installed wind and solar capacity, W and S, in W. The aim of this model is to provide a tool to investigate and predict the yearly bought and wasted energy, when designing the RES system, for a BS supply located in a given country.

First, for each country, we run multiple simulations, as described in section 4, to create a data-set used to build each model of each country. These simulations are performed with different values of W and S and for each pair of values for W and S, two different simulations are performed, one considering the traffic demand of the Train Station BS and the other the traffic demand of the San Siro BS. For each simulation, E_b and E_w are computed, so that a data-set for E_b and another for E_w are built. Each row of the E_b data-set contains the installed wind capacity W, the installed solar capacity S and the resulting E_b, when these capacities are employed to power the considered

BS. Similarly, in each entry of the E_w data-set, there are the employed capacities W and S and the obtained E_w. First, the statistical significant relations between W, S and our energy metrics E_b and E_w is verified. To do this, we use the p-value index. The p-value results for each country are reported in Table 2, presenting each value lower or equal to 0.5, confirming the existence of statistical relationships between these parameters.

We model this relationship as a second degree polynomial, as suggested by Fig. 4. For each country, receiving as input the solar and the wind capacity, S and W, the values of E_b and E_w are computed as follows:

$$E_b = a_b S + b_b W + c_b S^2 + d_b SW + e_b W^2 + K_b \quad (8)$$

$$E_w = a_w S + b_w W + c_w S^2 + d_w SW + e_w W^2 \quad (9)$$

where a_b, b_b, a_w and b_w are in Wh/W, c_b, d_b, e_b, c_w, d_w and e_w in Wh/W^2 and K_b in Wh. Each coefficient of each model is defined through the Linear Regression, using 66% of the corresponding data-set. The remaining 34% is employed as a test set for the model evaluation. Note that in the model of E_w, the constant term is not present, so that E_w is 0 MWh, when C_{tot} is

Table 4: Coefficients of the models for the prediction of E_w.

Country	a_w	b_w	c_w	d_w	e_w
Belgium	57.05	100.29	0.11	0.15	0.18
Denmark	-8.98	73.81	0.19	0.14	0.09
Germany	-83.70	-8.04	0.17	0.12	0.09
Switzerland	-56.00	-78.81	0.15	0.09	0.06

Table 5: R^2 and $NMRSE$ of the models used for E_b (R_b^2 and $NMRSE_b$, respectively) and E_w (R_w^2 and $NMRSE_w$, respectively), for each country.

Country	R_b^2	$NMRSE_b$	R_w^2	$NMRSE_w$
Belgium	0.97	0.08	0.99	0.07
Denmark	0.97	0.08	0.99	0.07
Germany	0.98	0.07	0.99	0.08
Switzerland	0.97	0.07	0.99	0.10

0 kW.

The resulting coefficients for E_b and E_w models are listed in Tables 3 and 4. In Table 5, each row reports R_b^2 and $NMRSE_b$, which are R^2 and $NMRSE$, computed on the test set, for the model of each country, to predict E_b. The table also gives R^2 and $NMRSE$ of the model for the E_w prediction, respectively R_w^2 and $NMRSE_w$. According to these values, these models predict E_b and E_w in at least 97% of the cases, as indicated by R^2 always larger or equal to 0.97, with an error never larger than 0.10.

The curve of models of E_b and E_w is shown in Figs. 6a, 6b, 6c, 6d, and 6e, 6f, 6g, 6h in Belgium, Denmark, Germany and Switzerland, respectively. First, we notice that the resulting model of E_b presents visible differences in Belgium with respect to the other countries. Indeed, in Belgium, the growth of the wind capacity W impacts more than the rise of the solar capacity S, as can be seen in Fig. 6a. In this model, the coefficients which multiply W, i.e., b_b and e_b, are larger, in absolute value, than, respectively a_b and c_b, which multiply S, making E_b more variable when that input parameter grows or decreases (see Table 3). Quite the opposite occurs for the other considered countries (see Figs. 6b, 6c and 6d). Indeed, in these cases, as reported in Table 3, the absolute values of b_b is always lower than a_b, as well as the one of e_b is always smaller than the one of c_b. This means that, for these countries, the variation of S affects more E_b than the W one. Similarly, for the E_w model, as can be seen in Table 4, e_w is larger than c_w, in the Belgian case, making it more affected by the variation of W than of S. Meanwhile, for the Danish, German and Swiss cases, e_w is lower than c_w, meaning that the grow or the drop of S impacts more E_w that the variation of W.

In Figs. 7a, 7b, 7c and 7d, each curve is computed

with the E_b model and represents E_b for a given C_{tot}, increasing the installed solar capacity S, while diminishing the wind capacity W. We notice that, while the Belgian case presents a growing trend (see 7a), for the other countries the trend is decreasing, as can be observed in Figs. 7b, 7c, 7d. This means that, according to the used data, for the supply of a BS, the wind capacity provides more usable energy than the solar, in Belgium, while quite the opposite occurs in Denmark, Germany and Switzerland. From these figures, we also notice that for C_{tot} large enough (larger than 2 kW), the hybrid solution is convenient, in terms of E_b and E_w, as in the simulation results, discussed in section 5.

7 CONCLUSIONS

In order to make RANs more sustainable and reduce the OPEX, a hybrid system, composed by a PV panel and a wind turbine, is considered for the BS supply, in addition to the electric grid. First, based on real data, we characterise the Belgian wind energy production, comparing it with the solar one. Results reveal that, while the solar production presents significant differences between daily and nightly hours, the nightly and daily wind generations are almost identical. Moreover, while the largest solar energy production occurs in summer, quite the opposite occurs for the wind energy production, which reaches its maximum production in winter. Hence, hybrid systems allow to better follow the BS demand with respect to single source systems. Indeed, simulation results reveal that the hybrid system supply provides significant reduction of the energy which needs to be bought from the grid. The presence of the turbine provides nightly energy supply to satisfy the small BS energy demand dur-
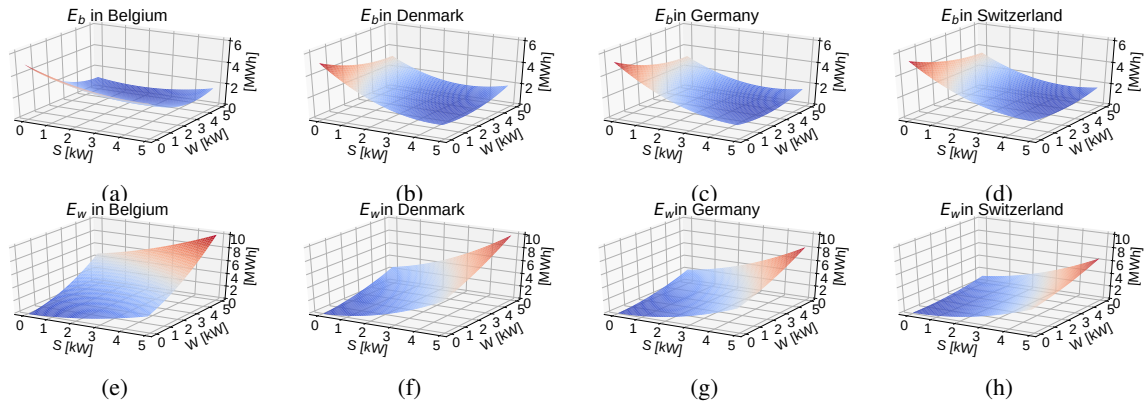
Figure 6: 3D shape of the models: (a) E_b model for Belgium, (b) E_b model for Denmark, (c) E_b model for Germany, (d) E_b model for Switzerland, (e) E_w model for Belgium, (f) E_w model for Denmark, (g) E_w model for Germany, (h) E_w model for Switzerland.
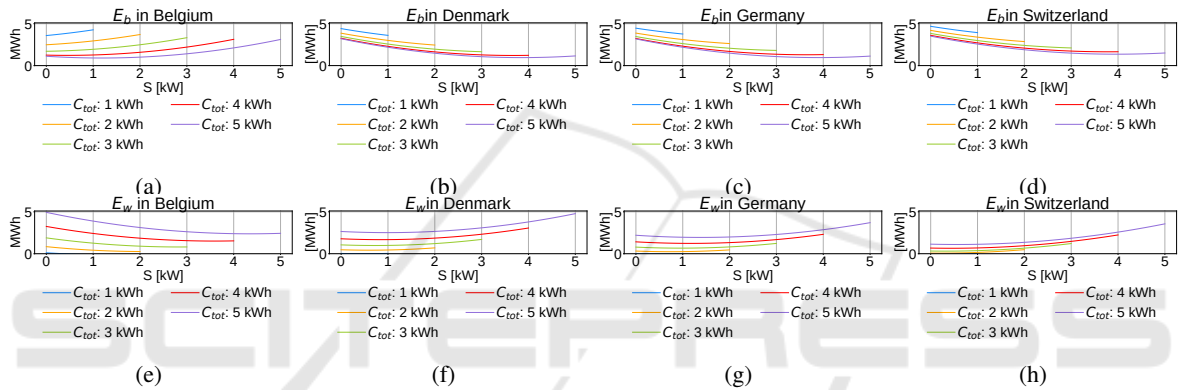

Figure 7: E_b and E_w provided by the model, for different C_{tot}, varying its distribution between solar and wind capacity: (a) E_b for Belgium, (b) E_b for Denmark, (c) E_b for Germany, (d) E_b for Switzerland, (e) E_w for Belgium, (f) E_w for Denmark, (g) E_w for Germany, (h) E_w for Switzerland.

ing the night and the PV panel guarantees the daily BS energy demand, which accounts for large values due to peak traffic demand that the turbine alone cannot satisfy. Finally, polynomial models for the energy performance prediction are built. These models highlight the different impact of the wind and solar capacities on the energy performance. In Belgium, the variation of the wind capacities impacts more than the solar one. Quite the opposite occurs in Denmark, Germany and Switzerland, where the impact of the solar capacity variation is larger than the one due to the wind turbine capacity variation.

REFERENCES

Aktar, M. R., Jahid, A., Hossain, M. F., and Al-Hasan, M. (2018). Energy sustainable traffic aware hybrid powered off-grid cloud radio access network. In *2018 International Conference on Innovations in Science, Engineering and Technology (ICISET)*, pages 121–125. IEEE.

Auer, G., Blume, O., Giannini, V., Godor, I., Imran, M., Jading, Y., Katranaras, E., Olsson, M., Sabella, D., Skillermark, P., et al. (2010). D2. 3: Energy efficiency analysis of the reference systems, areas of improvements and target breakdown. *Earth*, 20(10).

Belkhir, L. and Elmeligi, A. (2018). Assessing ict global emissions footprint: Trends to 2040 & recommendations. *Journal of Cleaner Production*, 177:448–463.

Bertoldi, P. (2017). Eu code of conduct on energy consumption of broadband equipment.

Bholowalia, P. and Kumar, A. (2014). Ebk-means: A clustering technique based on elbow method and k-means in wsn. *International Journal of Computer Applications*, 105(9).

Chamola, V. and Sikdar, B. (2016). Solar powered cellular base stations: Current scenario, issues and proposed solutions. *IEEE Communications magazine*, 54(5):108–114.

Commission, E. (2019). The european green deal com/2019/640 final.

Data, O. P. S. (2020). Data package time series.

Deruyck, M., Renga, D., Meo, M., Martens, L., and Joseph, W. (2017). Accounting for the varying supply of solar energy when designing wireless access networks.

IEEE Transactions on Green Communications and Networking, 2(1):275–290.

Desgraupes, B. (2013). Clustering indices. *University of Paris Ouest-Lab Modal'X*, 1:34.

Forecast, C. V. (2019). Cisco visual networking index: Forecast and trends, 2017–2022. *White paper, Cisco Public Information*.

Gati, A., Salem, F. E., Serrano, A. M. G., Marquet, D., Masson, S. L., Rivera, T., Phan-Huy, D.-T., Altman, Z., Landre, J.-B., Simon, O., et al. (2019). Key technologies to accelerate the ict green evolution–an operator's point of view. *arXiv preprint arXiv:1903.09627*.

Guo, S., Zeng, D., Gu, L., and Luo, J. (2019). When green energy meets cloud radio access network: Joint optimization towards brown energy minimization. *Mobile Networks and Applications*, 24(3):962–970.

Hadji, F., Ihaddadene, N., Ihaddadene, R., Kherbiche, Y., Mostefaoui, M., and Beghidja, A. H. (2018). Solar energy in m'sila (algerian province). In *2018 6th International Renewable and Sustainable Energy Conference (IRSEC)*, pages 1–5. IEEE.

Han, T. and Ansari, N. (2014). Powering mobile networks with green energy. *IEEE Wireless Communications*, 21(1):90–96.

Hassan, H. A. H., Nuaymi, L., and Pelov, A. (2013). Renewable energy in cellular networks: A survey. In *2013 IEEE online conference on green communications (OnlineGreenComm)*, pages 1–7. IEEE.

Hirsch, R. L. (2008). Mitigation of maximum world oil production: Shortage scenarios. *Energy policy*, 36(2):881–889.

IEA (2020). World energy outlook 2020.

Kodinariya, T. M. and Makwana, P. R. (2013). Review on determining number of cluster in k-means clustering. *International Journal*, 1(6):90–95.

Petrovic, S. (2006). A comparison between the silhouette index and the davies-bouldin index in labelling ids clusters. In *Proceedings of the 11th Nordic Workshop of Secure IT Systems*, pages 53–64. Citeseer.

Pompili, D., Hajisami, A., and Tran, T. X. (2016). Elastic resource utilization framework for high capacity and energy efficiency in cloud ran. *IEEE Communications Magazine*, 54(1):26–32.

Renga, D., Hassan, H. A. H., Meo, M., and Nuaymi, L. (2018). Energy management and base station on/off switching in green mobile networks for offering ancillary services. *IEEE Transactions on Green Communications and Networking*, 2(3):868–880.

Renga, D. and Meo, M. (2019). Dimensioning renewable energy systems to power mobile networks. *IEEE Transactions on Green Communications and Networking*, 3(2):366–380.

Res., P. (2013). Off-grid power for mobile base stations—renewable and alternative energy sources for remote mobile telecommunications: Global market analysis and forecasts.

Smertnik, H. et al. (2014). Green power for mobile bi-annual report. *GSM Association, August*, 12(31):181.

Tariq, F., Khandaker, M. R., Wong, K.-K., Imran, M. A., Bennis, M., and Debbah, M. (2020). A speculative study on 6g. *IEEE Wireless Communications*, 27(4):118–125.